Fingering inside the coffee ring

Byung Mook Weon* and Jung Ho Je†

X-ray Imaging Center, Department of Materials Science and Engineering, Pohang University of Science and Technology, San 31, Hyoja-dong, Pohang 790-784, Korea

(Received 24 September 2012; revised manuscript received 13 November 2012; published 3 January 2013)

Colloidal droplets including micro- and nanoparticles generally leave a ringlike stain, called the "coffee ring," after evaporation. We show that fingering emerges during evaporation inside the coffee ring, resulting from a bidispersed colloidal mixture of micro- and nanoparticles. Microscopic observations suggest that finger formation is driven by competition between the coffee-ring and Marangoni effects, especially when the inward Marangoni flow is overwhelmed by the outward coffee-ring flow. This finding could help to understand the variety of the final deposition patterns of colloidal droplets.

DOI: 10.1103/PhysRevE.87.013003 PACS number(s): 47.57.J−, 47.54.−r, 47.55.np, 64.70.fm

I. INTRODUCTION

When a drop of colloidal fluid, such as coffee or a colloidal suspension, dries on a solid surface, the evaporating liquid pushes the suspended colloids to the drop edge, concentrating them and leaving a ringlike deposit. The coffee ring is usually induced by edgeward capillary flows [1–3]. The evaporating liquid is cooled by heat loss, resulting in temperature or surface tension gradients along the liquid surface. These gradients lead to surface-tension-induced flows in what is known as the Marangoni effect [4–6]. In addition, the motion of the edgeward colloids can be halted if the colloids come in contact with the liquid surface because a net capillary force can push the colloids to the drop center as the contact angle decreases over time [7]. The Marangoni and capillary force effects can effectively reverse the coffee-ring effect and influence the final deposition patterns, which are important in applications such as self-assembly [7] and ink-jet printing [8]. The suppression of the coffee-ring effect is an important technological issue [9,10]. However, the competitive and cooperative interactions between the coffee-ring effect and the Marangoni and/or capillary force effects are not fully understood.

This paper shows an unexpected fingering inside the coffee ring. We found fingerlike patterns inside the ringlike stains during the evaporation of colloidal drops of a bidispersed mixture of micro- and nanoparticles. Real-time confocal microscopic observations suggest that finger formation is driven by the interaction between the coffee-ring and Marangoni effects. This finding has implications for predicting the final deposition patterns of colloidal fluids and for improving inkjet printing [8,11,12], particle separation [7,13,14], and drying-mediated self-assembly technologies [15,16].

To understand the variety of the final deposition patterns, it would be better to consider feasible variations of particle motion induced by contact-line evaporation as illustrated in Fig. 1(a). The coffee-ring flow is directed *outward* and the reversal flows caused by the Marangoni and capillary force effects are directed *inward*. The Marangoni flow is directed inward along the liquid surface if the thermal conductivity ratio between the substrate and the liquid (k_R) is greater than 2 [5], and the capillary force effect induces inward particle movement by the droplet geometry [7]. Decalin droplets deposited on glass slides have a k_R value ≈10, indicating the possibility of interactions among the three effects.

II. EXPERIMENTAL METHODS

The decalin/glass configuration is useful for studying the Marangoni effect because it shows an inward Marangoni flow along the liquid/air interface resulting from $k_R = k_S/k_L > 2$, the ratio of the thermal conductivities of the substrate and liquid [5]. The k_R of decalin on glass is ≈10 ($k_{\mathrm{dec}} = 0.14$ W/m K [17] and $k_{\mathrm{glass}} = 1.38$ W/m K [6]) [Fig. 1(a)], which is comparable to the value for octane on glass ($k_R \approx 8$) [4,5]. As a result of the slow evaporation kinetics of decalin, the humidity effect can be disregarded because of a small vapor pressure $p_v = 120$ Pa, which is equivalent to the saturation vapor density $c_v \approx 6.5$ g/m^3 [18]. The material properties of decalin at room temperature are as follows: density $\rho \approx 897$ kg/m^3 [7,19], dynamic viscosity $\eta \approx 3 \times 10^{-3}$ Pa s [18], temperature dependence of the surface tension $\beta = -d\gamma/dT \approx 1 \times 10^{-4}$ N/(m·K) [18], latent heat of vaporization $L \approx 300$ J/g [20], and vapor diffusivity in air $D \approx 5 \times 10^{-6}$ m^2/s [21].

Decalin-based colloidal fluids have been extensively studied as model hard-sphere systems [18]. In this study, the poly(methyl methacrylate) (PMMA) colloids were stabilized by a thin (10–20 nm) grafted layer of poly(12-hydroxystearic acid) (PHSA), synthesized by Schofield [22]. The colloid radii were $r_S = 0.1$ μm (nanospheres) and $r_L = 1$ μm (microspheres) with ∼5% polydispersity in size, as determined by dynamic light scattering (ALV 5000, 532 nm laser, 90° scattering angle). This bidispersed mixture is useful for studying different coffee stains [13]. The PMMA colloids (density $\rho_{\mathrm{PMMA}} = 1190$ kg/m^3; refractive index $n_{\mathrm{PMMA}} = 1.49$) were evenly suspended in decalin (a mixture of *cis*- and *trans*-decalin, $\rho_{\mathrm{dec}} = 897$ kg/m^3 and $n_{\mathrm{dec}} = 1.48$) [7].

To identify the colloidal particle motions with confocal microscopy, we used fluorescently labeled colloids suspended in unlabeled decalin. The motions of the fluorescently labeled PMMA colloids in decalin drops on precleaned micro cover glass (VWR, 22 × 30 mm^2, No. 1.5) were clearly visualized in

*bmweon@hotmail.com
†jhje@postech.ac.kr

 ©2013 American Physical Society

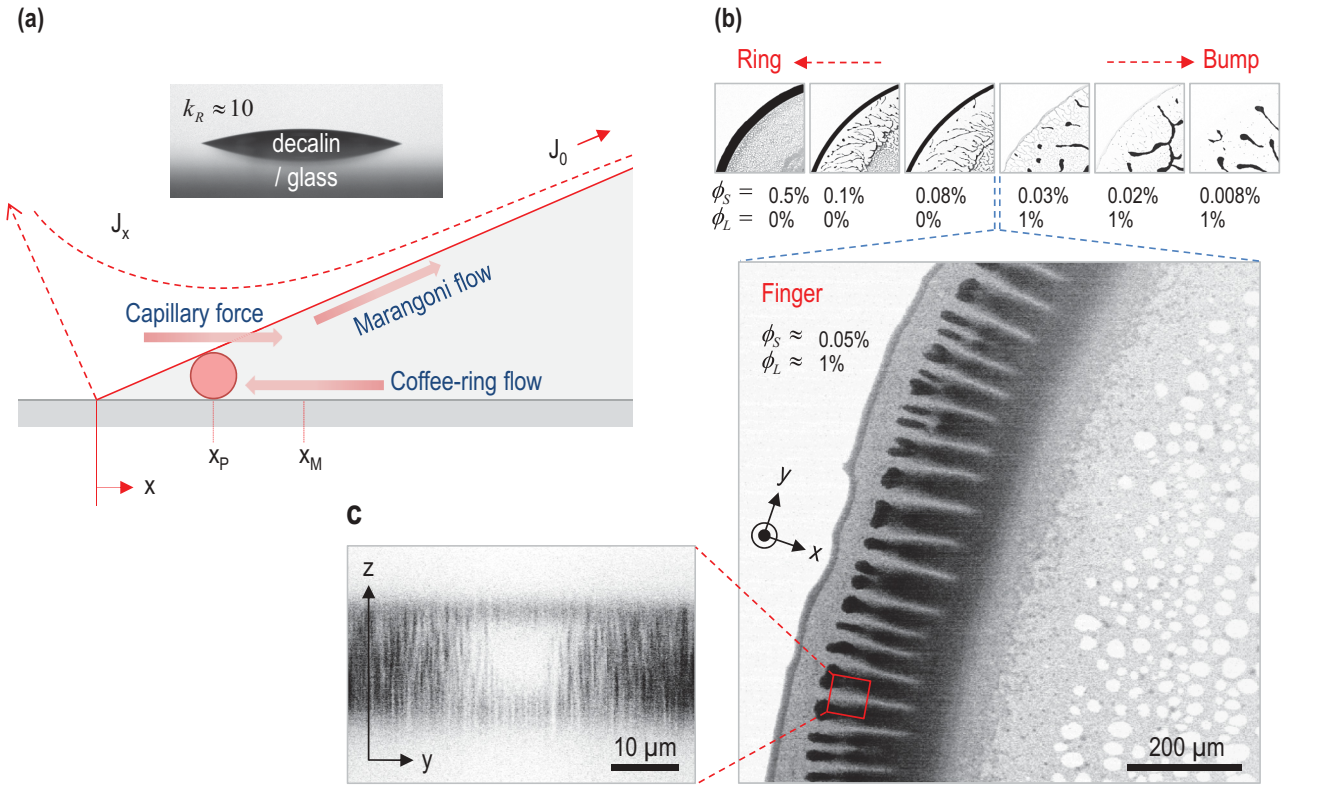

FIG. 1. (Color online) (a) The coffee-ring flow is induced by the divergence of the vapor flux J, where J_0 is the flux at the drop center. The Marangoni flow is induced by evaporative cooling and is directed inward along the liquid surface [$k_R \approx 10$ (the thermal conductivity ratio between the substrate and the liquid) for decalin on glass [26]. The capillary force effect is induced by contact between the outermost colloids and the liquid surface. The outermost particle position (x_P) and the stagnation point (x_M), where the direction of the Marangoni flow is inverted, are important for identifying the particle size effect. (b) Representative confocal microscopy images (911 × 911 μm^2) of the final deposition patterns from 0.5 μl drops of colloidal fluids on glass. Small colloids with $r_S = 0.1$ μm and volume fractions $\phi_S = 0.1\%-1\%$ tended to form edge rings (Movies S1 and S2 [26]), whereas large colloids with $r_L = 1.0$ μm and $\phi_L = 0.1\%-1\%$ formed bumps (Movies S3 and S4 [26]). Fingers were observed for bidispersed colloids ($\phi_S \approx 0.05\%$ and $\phi_L \approx 1\%$). (c) Cross-sectional confocal image for a single finger, showing a finger thickness of ~20 μm.

real time by a confocal microscope (Leica TCS SP5) [7] with an oil immersion objective of 100 × 1.4 numerical aperture, an Ar+ laser excitation of 488 nm, and a TD488/543/633 detector with a PMT1 of 500−570 nm. The typical image size was 512 × 512 pixels, corresponding to 911 × 911 μm^2.

III. EVAPORATION-INDUCED EFFECTS

The coffee-ring effect is relevant to the evaporative vapor flux divergence at the drop edge. The vapor flux J diffusing from the free surface of the liquid to the air diverges significantly at the thin edge [1–3] and can be described as $J = J_0(x/R)^{-\lambda}$ with $\lambda = (\pi - 2\theta)/(2\pi - 2\theta)$, where x is the radial position from the contact line of a drop with a radius R and a contact angle θ and λ is the characteristic angular function. Note that λ depends slightly on θ. The prefactor J_0, which indicates the vapor flux at the drop center, depends on the vapor diffusivity into the air D, the saturation vapor density difference Δc from the liquid surface (c_s) to infinity (c_∞) (for weak volatile liquids, $\Delta c \approx c_s$ and $c_\infty \approx 0$), and the droplet geometry (i.e., R and θ) [3]. The diverged flux causes the fluid to carry the suspended colloidal particles toward the edge, forming the ring deposits [1]. Conversely, the particles' outward motion stops at a position x_P where the particle diameter $2r$ is equal to the height of the liquid surface, $x_P \tan\theta$ [7,13,14,23]. The capillary force effect is more important for larger particles and is mainly governed by the outermost particle position x_P, and thus the vapor flux $J/J_0 = (x_P/R)^{-\lambda}$ [modified from [1] with $J \sim (R-r)^{-\lambda}$ and $J_0 \sim R^{-\lambda}$; $x_P = (R-r)$, where r is the distance from the edge].

The Marangoni effect is induced by evaporative cooling. The vapor flux contributes to the heat loss rate per unit area at the drop center, $Q_{\text{evap}} = J_0 L$, where L is the latent heat of vaporization [24]. The heat loss is balanced with the heat flux through the liquid layer, with the drop height h_0 at the drop center and a liquid thermal conductivity of k_L, as given by $Q_{\text{cond}} = k_L \Delta T_0 / h_0$ [24], where the temperature difference ΔT_0 at the drop center from the liquid surface to the substrate is assumed to be equal to the local temperature difference $\Delta T_{c\text{-}e}$ along the liquid surface from the center to the edge [5,6]. Here, $\Delta T_0 = \Delta T_{c\text{-}e} = J_0 L h_0 / k_L$, which is obtained by setting $Q_{\text{evap}} = Q_{\text{cond}}$, alters the liquid surface tension γ, as described by the temperature dependence of the surface tension $\beta = -d\gamma/dT$, where $d\gamma/dT$ is negative for most liquids [5,6]. The surface tension change induces the

Marangoni stress, which leads to Marangoni flow from a warm region to a cooler region [5,6]. The reversal of the Marangoni flow is determined not only by the thermal conductivity ratio between the substrate and the liquid but also by the local film thickness [5]. At a stagnation point, denoted by x_M, the direction of the Marangoni flow can be locally changed when the local temperature difference ΔT along the liquid surface is at a local minimum as $d\Delta T/dx \to 0$, corresponding to $d\gamma/(\beta dx) = 0$ or $d\gamma/dx = 0$ because $\beta = -d\gamma/dT$. This local point is given as $x_M = [2\lambda/(2-\lambda)(h_f R_f)]^{1/2}$ (taken from [25]), where h_f is the thickness of the adsorbed liquid film and R_f is the radius of the liquid surface adjacent to the flat adsorbed film [25]. By adopting values of $h_f \approx 100$ nm and $R_f \approx 1$ mm for water [25], the stagnation point for decalin is assumed to be at $x_M \approx 10\,\mu$m, which is almost independent of the droplet geometry (λ or θ) and the particle deposition.

IV. RESULTS

We observed the evaporation dynamics of decalin drops on a clean glass substrate using confocal microscopy [26]. The drops contained uniformly distributed poly(methyl methacrylate) colloidal particles that were labeled with a fluorescent dye. Once the drops were pinned by particle accumulation [27], the contact angles decreased linearly with time during the evaporation process [28]. The typical deposition patterns [Fig. 1(b)], which include the ring, bump, and finger patterns, depend on the particle volume fractions (ϕ) and combinations of small or large colloids (ϕ_S or $\phi_L = 0\%-1\%$). The initial drop volume was 0.5 μl, resulting from the initial contact radius $R_0 \approx 1.4$ mm and the initial contact angle $\theta_0 \approx 15^\circ$ for monodispersed (small or large) colloids. For bidispersed colloids, the values were $R_0 \approx 1.2$ mm and $\theta_0 \approx 20^\circ$ [26]. Given a high size ratio ($r_L/r_S \approx 10$), small colloids easily pass through the interstices of large colloids. We observed that small colloids preferentially moved to the edge, leaving edgeward *rings* (Movie S1 for $\phi_S = 0.1\%$ and Movie S2 for $\phi_S = 1\%$ [26]), while large colloids left centerward *bumps* (Movie S3 for $\phi_L = 0.1\%$ and Movie S4 for $\phi_L = 1\%$ [26]). For monodispersed colloids, a larger volume fraction and a smaller particle radius favor contact-line pinning and, thus, ring formation [29]. The edge rings made of colloids are closely packed and the rigidness of the rings is reinforced by particle accumulation [2], jamming [27], or crystallization [30]. For a specific condition of bidispersed colloids ($\phi_S \approx 0.05\%$ and $\phi_L \approx 1\%$), we observed *fingerlike patterns*, as clearly shown in Fig. 1(b). Each finger has a thickness of $\sim$20 μm [Fig. 1(c)]. Therefore, the mixing of small and large colloids must be important to fingering pattern formation.

The sequential snapshots (Fig. 2; Movie S5 [26]) with real-time confocal microscopic observations show that small colloids formed the outer ring, whereas large colloids formed the inner ring. The inner ring position, measured by averaging the front and rear positions, scales as $x_P\,(\mu\text{m}) \approx 432.6(t/t_f) - 174.1$, where the complete evaporation time t_f($\approx$2465 s) was measured with confocal imaging. This linear scaling is quite different from the $(1-t/t_f)^{-1}$ scaling resulting from the capillary force effect [7]. Interestingly, we observed that fingering appeared at $t/t_f \approx 0.6$ when the droplet contact angle became as small as $\theta \approx 8.1^\circ$ (Fig. 2).

Once a finger formed at $t/t_f \approx 0.6$, the finger height increased with ring width. The measured front positions, taken from Fig. 2, increased with time as shown in Fig. 3(a), whereas the rear positions were approximately fixed after 1380 s ($t/t_f \approx 0.56$). The fixation of the rear position was attributed to the rigid packing of large colloids. The growth of the inner ring widths at 1440 s ($t/t_f \approx 0.6$) [Fig. 3(b)], taken from the difference between the front and rear positions [Fig. 3(a)], matched the growth of the finger heights [Fig. 3(b)], taken from

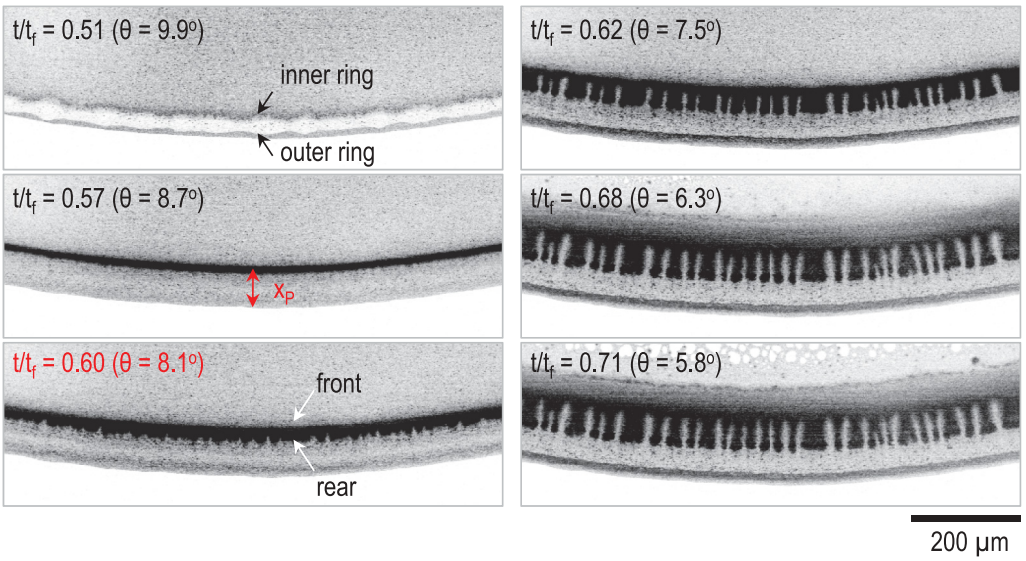

FIG. 2. (Color online) For bidispersed colloids ($\phi_S \approx 0.05\%$ and $\phi_L \approx 1\%$; Movie S5 [26]), sequential confocal images of a 0.5 μl decalin drop ($R_0 \approx 1.2$ mm and $\theta_0 \approx 20^\circ$) on glass show that the small colloids formed the outer ring, whereas the large colloids formed the inner ring. The inner ring position (x_P), which is the average of the front and rear positions, gradually shifted to the center. Once the fingers were generated after $t/t_f > 0.6$ ($\theta_c = 8.1^\circ$), they grew as the inner ring width increased by coffee-ring-driven particle deposition.

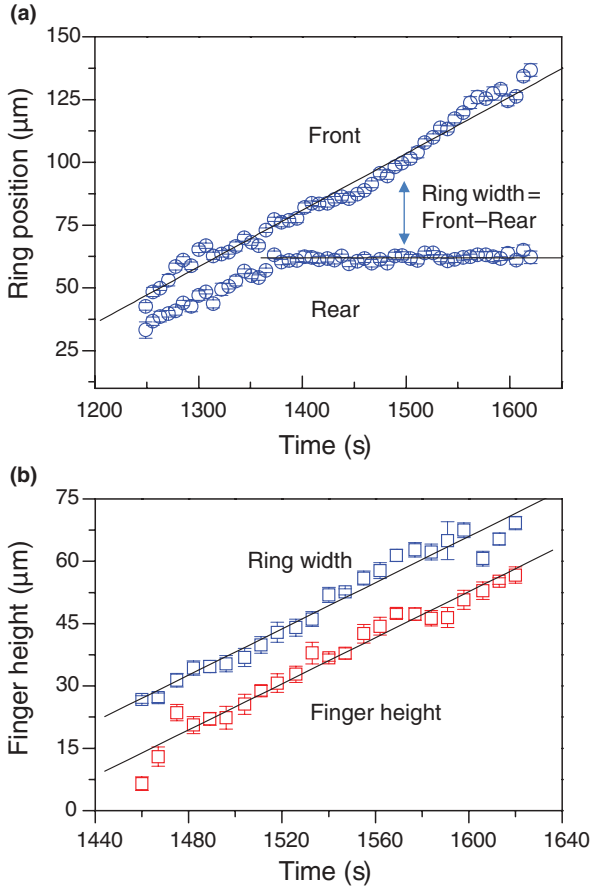

FIG. 3. (Color online) (a) The evolutions of the front and rear positions of the inner ring show that the front grew continually whereas the rear halted after 1380 s ($t/t_f \approx 0.56$, $t_f = 2465$ s). The ring width was defined as the difference between the front and rear positions. (b) The correlation between the ring width and the finger height suggests that the finger growth originated from the ring width, driven by the coffee-ring effect.

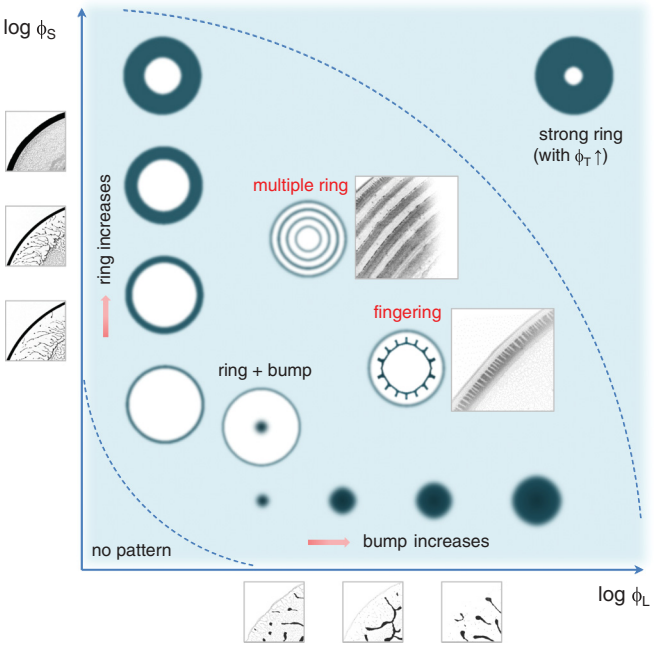

FIG. 4. (Color online) Schematic phase diagram guides us to possible phase spaces for the ring, bump, and finger formations, with the particle volume fractions corresponding to large and small colloids (ϕ_L and ϕ_S, respectively) for a fixed droplet radius.

Fig. 2. This correlation between the ring widths and the finger heights suggests that finger growth is related to ring growth, which results from the interaction between the coffee-ring and Marangoni flows.

The schematic phase diagram in Fig. 4 illustrates possible phase spaces for the ring, bump, and finger formations for particle volume fractions corresponding to large and small colloids (ϕ_L and ϕ_S, respectively). For small (large) colloids, ring (bump) patterns increase with ϕ_S (ϕ_L). At high concentrations, $\phi_T = \phi_S + \phi_L$, a strong ring is expected. The fingering in decalin is attributed to competition between the coffee-ring and Marangoni effects intermediate between ϕ_S and ϕ_L, respectively, consistent with the images in Fig. 1(b). Multiple rings may form given a mixture of conditions and the formation mechanism of multiple rings is related to particle separation by size [7].

V. DISCUSSION

The outward coffee-ring flow, which is initially independent of the inward Marangoni flow, becomes competitive with the Marangoni flow when the droplet contact angle is sufficiently lower than a critical angle. To understand the competition between the capillary and Marangoni flows, it would be useful to compare their flow velocities. The coffee-ring velocity is known to scale as $V_C = J/\rho$, where J is the vapor flux diffusing from the free surface of the liquid to the air and ρ is the liquid density [31,32]. The Marangoni velocity is known to scale as $V_M = (1/32)\beta\theta^2\Delta T_0/\eta$, where θ is the droplet contact angle, $\beta = -d\gamma/dT$ is the temperature dependence of the surface tension, ΔT_0 is the temperature difference at the drop center from the liquid surface to the substrate, and η is the liquid dynamic viscosity [31,32]. The velocity ratio of the two flows can be expressed as

$$V_C/V_M = \omega(J/J_0)/(\theta^2 h_0).$$

Here $\omega = 32\eta k_L/(\beta\rho L)$ is a characteristic length (e.g., $\omega \approx 493$ nm for decalin and $\omega \approx 112$ nm for octane; Table I) associated only with the liquid properties [η, k_L (the thermal conductivity), β, ρ, and L (the latent heat of vaporization)]; $J/J_0 = (R/x_P)^\lambda$ [modified from [1] with $J \sim (R-r)^{-\lambda}$ and $J_0 \sim R^{-\lambda}$; $x_P = (R-r)$] is a function of the droplet contact radius R, the outermost particle position x_P, and $\lambda = (\pi - 2\theta)/(2\pi - 2\theta)$; and $\theta^2 h_0$ is the geometric factor with the droplet height h_0 at the droplet center. The ω value is important to evaluate the possibility of transition from Marangoni dominance to coffee-ring dominance. At a given ω value, there is a critical angle $\theta_c = [(\omega/h_0)(J/J_0)]^{1/2}$ for a condition of $V_C = V_M$. The critical angle would usefully imply that when the droplet contact angle decreases below θ_c during evaporation, the coffee-ring effect can dominate over the Marangoni effect.

We note that most water-based experiments do not report fingering pattern formation. For water on glass, the deposition

TABLE I. Estimation of ω values. The $\omega = 32\eta k_L/(\beta\rho L)$ value is a characteristic length constant, associated only with the liquid properties (the dynamic viscosity η, the thermal conductivity k_L, the temperature dependence of the surface tension $\beta = -d\gamma/dT$, the liquid density ρ, and the latent heat of vaporization L). This characteristic value determines the critical contact angle $\theta_c = [(\omega/h_0)(J/J_0)]^{1/2}$ between the coffee-ring dominance and the Marangoni dominance ($V_C = V_M$). The estimation results for typical liquids are based on liquid properties from the literature.

Factor	Unit	Decalin	Dodecane	Decane	Octane	Toluene	Hexane	Water
η	mPa s	3.0	1.34	0.92	0.54	0.56	0.294	0.894
k_L	J/s m K	0.14	0.14	0.15	0.13	0.13	0.12	0.58
β	mN/m K	0.1	0.0884	0.092	0.0951	0.119	0.102	0.168
ρ	kg/m^3	900	800	700	700	900	700	1000
L	J/g	300	256	263	300	300	365	2400
ω	nm	493	351	246	112	76	48	41

patterns are either rings for small colloids [1] or bumps for large colloids [7]. The lack of fingering in water can be explained in terms of the suppression of the Marangoni flow in water [1,4,25]. Comparison of octane and decalin is more informative: fingering is not observed in octane [4] but is observed in decalin. The difference between octane and decalin can be explained by the characteristic length constant (ω) or the relevant critical contact angle (θ_c). For decalin, the critical angle was estimated from the droplet height (h_0) and the relative evaporative flux (J/J_0) at $t/t_f \approx 0.6$. This angle is high in decalin ($\theta_c \approx 8.3^\circ$) for bidispersed colloids because of its high ω value, implying coffee-ring dominance and the creation of a variety of formations, such as bumps or fingers. However, for octane and its low ω values, no transition from Marangoni dominance to coffee-ring dominance is expected because of its small θ_c. For an octane drop with $R_0 = 2.0$ mm and $\theta_0 = 50^\circ$, $\theta_c \approx 0$ [4]. Thus, the Marangoni effect always overwhelms the coffee-ring effect for most drop lifetimes. As a result, only bumps can be formed in octane under Marangoni dominance [4,5]. Decalin's characteristic length constant of $\omega = 493$ nm is much higher than that of most other liquids, including octane ($\omega = 112$ nm) (Table I). This consideration suggests that higher ω values or higher critical contact angles are more favorable for finger pattern formation.

Small colloids primarily contributed to the edgeward *rings* [Fig. 1(b)]. This trend provides an important insight into the effect of particle size: the motion of small colloids is driven mainly by the coffee-ring flow. This situation is plausible given $x_P < x_M$, where x_M is the stagnation point for a local minimum in the temperature difference, which results in a high J/J_0 ratio and $V_C > V_M$. This condition allows the preferential segregation of small colloids at the edge [1,2,6]. For large colloids, the Marangoni or capillary force effect can substantially reverse the coffee-ring effect, as illustrated in Fig. 1(a). The sequential snapshots (Movie S6 [26]) of large colloids ($r_L = 1$ μm and $\phi_L = 0.1\%$) show that the colloids initially moved to the edge and then returned to the center. The temporal evolution of the ring position (x_P), taken from the outermost colloids, shows that the colloids moved toward the center from $t/t_f > 0.3$, matching the capillary force scaling of $x_P = (2r/\theta_0)(1 - t/t_f)^{-1}$ [7]. This result suggests that the capillary force effect can reverse the coffee-ring effect if the Marangoni effect is disregarded.

The fingering inside the coffee ring occurs at a specific mixture of micro- and nanoparticles and is quite different from the particle segregation effect of colloidal droplets [7,13,14,28,33]. The large particle motion may be different from the small particle motion even under the same flow velocities [13]. A more exact expression of the flow velocities (e.g., [30]) would be helpful to identify the particle effects. The fluorophore may act as a surfactant on the colloids used for confocal microscopy [34], perhaps altering the Marangoni effect with the particle concentration [35]. The particle pinning at the contact line and the contact-line movement depend on the particle size and concentration, influencing the particle motion by inducing a net capillary force [36], where the particle/air interfacial tension [37] may be important. The small particles are easily packed at the contact line by the coffee-ring flow, while the large particles are affected by the Marangoni flow. The transition from the Marangoni effect to the coffee-ring effect would be feasible in their mixture. Further study is needed to understand the profound effects of the particle size and concentration.

VI. CONCLUSION

In conclusion, modern printing technology with colloids on a solid or flexible substrate requires a better understanding of coffee-ring-related effects. The microscopic observations suggest that the fingering for specific bidispersed colloids is induced by the interaction between the coffee-ring and Marangoni effects, when the inward Marangoni flow is overwhelmed by the outward coffee-ring flow. The transition from the Marangoni effect to the coffee-ring effect can be evaluated by adopting a critical droplet contact angle. The fingering inside the coffee ring is not general but possible when the critical contact angle is high and in a specific colloidal mixture. The physical constraints that determine the final deposition patterns are important to control the deposition patterns formed from evaporating colloidal fluids.

ACKNOWLEDGMENT

This research was supported by the Creative Research Initiatives (Functional X-ray Imaging) of MEST/NRF.

[1] R. D. Deegan, O. Bakajin, T. F. Dupont, G. Huber, S. R. Nagel, and T. A. Witten, Nature (London) **389**, 827 (1997).
[2] R. D. Deegan, O. Bakajin, T. F. Dupont, G. Huber, S. R. Nagel, and T. A. Witten, Phys. Rev. E **62**, 756 (2000).
[3] H. Hu and R. G. Larson, J. Phys. Chem. B **106**, 1334 (2002).
[4] H. Hu and R. G. Larson, J. Phys. Chem. B **110**, 7090 (2006).
[5] W. D. Ristenpart, P. G. Kim, C. Domingues, J. Wan, and H. A. Stone, Phys. Rev. Lett. **99**, 234502 (2007).
[6] R. Bhardwaj, X. Fang, and D. Attinger, New J. Phys. **11**, 075020 (2009).
[7] B. M. Weon and J. H. Je, Phys. Rev. E **82**, 015305 (2010).
[8] M. Shih, H. M. Haverinen, P. Dhagat, and G. E. Jabbour, Adv. Mater. **22**, 673 (2010).
[9] P. J. Yunker, T. Still, M. A. Lohr, and A. G. Yodh, Nature (London) **476**, 308 (2011).
[10] H. B. Eral, D. M. Augustine, M. H. G. Duits, and F. Mugele, Soft Matter **7**, 4954 (2011).
[11] J. A. Liddle, Nat. Nanotechnol. **2**, 533 (2007).
[12] H. Minemawari, T. Yamada, H. Matusui, J. Tsutsumi, S. Hass, R. Chiba, R. Kumai, and T. Hasegawa, Nature (London) **475**, 364 (2011).
[13] V. H. Chhasatia and Y. Sun, Soft Matter **7**, 10135 (2011).
[14] T. S. Wong, T. H. Chen, X. Shen, and C. M. Ho, Anal. Chem. **83**, 1871 (2011).
[15] E. Rabani, D. R. Reichman, P. L. Geissler, and L. E. Brus, Nature (London) **426**, 271 (2003).
[16] W. Han and Z. Lin, Angew. Chem., Int. Ed. **50**, 2 (2011).
[17] D. Frezzotti, G. Goffredi, and E. Bencini, Thermochim. Acta **265**, 119 (1995).
[18] J. Leng, Phys. Rev. E **82**, 021405 (2010).
[19] J. S. Lee, B. M. Weon, S. J. Park, J. H. Je, K. Fezzaa, and W. K. Lee, Nat. Commun. **2**, 367 (2011).
[20] G. F. Davies and E. C. Gilbert, J. Am. Chem. Soc. **63**, 1585 (1941).
[21] N. F. Dubovkin and L. N. Smirnova, Chem. Technol. Fuels Oils **16**, 255 (1980).
[22] A. Schofield, http://www.ph.ed.ac.uk/∼abs/
[23] X. Shen, C. M. Ho, and T. S. Wong, J. Phys. Chem. B **114**, 5269 (2010).
[24] L. Y. Barash, T. P. Bigioni, V. M. Vinokur, and L. N. Shchur, Phys. Rev. E **79**, 046301 (2009).
[25] X. Xu and J. Luo, Appl. Phys. Lett. **91**, 124102 (2007).
[26] See Supplemental Material at http://link.aps.org/supplemental/10.1103/PhysRevE.87.013003 for the confocal microscopic movies.
[27] R. D. Deegan, Phys. Rev. E **61**, 475 (2000).
[28] B. M. Weon, J. H. Je, and C. Poulard, AIP Adv. **1**, 012102 (2011).
[29] A. S. Sangani, C. Lu, K. Su, and J. A. Schwarz, Phys. Rev. E **80**, 011603 (2009).
[30] A. G. Marin, H. Gelderblom, D. Lohse, and J. H. Snoeijer, Phys. Rev. Lett. **107**, 085502 (2011).
[31] H. Hu and R. G. Larson, Langmuir **21**, 3963 (2005); **21**, 3972 (2005).
[32] R. Bhardwaj, X. Fang, P. Somasundaran, and D. Attinger, Langmuir **26**, 7833 (2010).
[33] C. Monteux and F. Lequeux, Langmuir **27**, 2917 (2011).
[34] J. H. J. Thijssen, A. B. Schofield, and P. S. Clegg, Soft Matter **7**, 7965 (2011).
[35] T. Still, P. J. Yunker, and A. G. Yodh, Langmuir **28**, 4984 (2012).
[36] B. M. Weon and J. H. Je, Phys. Rev. Lett. (in press).
[37] B. M. Weon, J. S. Lee, J. T. Kim, J. Pyo, and J. H. Je, Curr. Opin. Colloid Interface Sci. **17**, 388 (2012).